



A Passivity-Based Stability Analysis of the Active Damping Technique in the Offshore Wind Farm Applications

Chen, Hsin Chih; Cheng, Po Tai; Wang, Xiongfei

Published in:

IEEE Transactions on Industry Applications

DOI (link to publication from Publisher):

[10.1109/TIA.2018.2853044](https://doi.org/10.1109/TIA.2018.2853044)

Publication date:

2018

Document Version

Accepted author manuscript, peer reviewed version

[Link to publication from Aalborg University](#)

Citation for published version (APA):

Chen, H. C., Cheng, P. T., & Wang, X. (2018). A Passivity-Based Stability Analysis of the Active Damping Technique in the Offshore Wind Farm Applications. *IEEE Transactions on Industry Applications*, 54(5), 5074-5082. Article 8403287. <https://doi.org/10.1109/TIA.2018.2853044>

General rights

Copyright and moral rights for the publications made accessible in the public portal are retained by the authors and/or other copyright owners and it is a condition of accessing publications that users recognise and abide by the legal requirements associated with these rights.

- Users may download and print one copy of any publication from the public portal for the purpose of private study or research.
- You may not further distribute the material or use it for any profit-making activity or commercial gain
- You may freely distribute the URL identifying the publication in the public portal -

Take down policy

If you believe that this document breaches copyright please contact us at vbn@aub.aau.dk providing details, and we will remove access to the work immediately and investigate your claim.

A Passivity-based Stability Analysis of the Active Damping Technique in the Offshore Wind Farm Applications

Hsin-chih Chen*, Po-tai Cheng*, Xiongfei Wang**, and Frede Blaabjerg**

(*)Center for Advanced Power Technologies, Department of Electrical Engineering,
National Tsing Hua University, Hsinchu, Taiwan

(**)Department of Energy Technique, Aalborg University, 9220 Aalborg East, Denmark

Abstract—The LCL-based filter has been widely applied to mitigate the size of the inductor in the high power converter, but it usually leads to resonance in the system. Therefore, an active damping technique based on the virtual resistor is provided in this paper for the LCL-filter system. Literature papers only suppressed the resonance of the LCL-filter and focused on the stability of the internal current control loop with an inductive grid impedance. Therefore, these previous stability analysis methods cannot be suitable for offshore wind farm applications due to the multiple resonance frequency characteristic of the transmission cable and multi-paralleled converters. Therefore, this paper analyzes the control stability with both of the internal resonance (LCL-filter) and external resonance (between the grid impedance and current controller). Besides, the behavior of multi-paralleled converter and the multiple resonance frequency of long transmission cable are discussed and analyzed for the offshore wind farm applications. Finally, the laboratory and simulation results are for the proposed method verification.

Index Terms—Active damping, LCL filter, multi-paralleled converter, passivity-based analysis, resonance

I. INTRODUCTION

The high power offshore wind farms have been popular to reduce the petrochemical energy in recent years. As the power density of wind power converters become higher, the LCL-filter is widely employed in the power electronic voltage source converters (VSCs) to reduce the size of the filter inductor and the switching frequency [1], [2]. However, the resonance characteristic of the LCL-filter usually results in huge and uncontrollable output current distortion even shut down the system operation. The additional resistor is a conventional method to prevent the resonance, but it significantly increases the power loss in the system [2], [3]. Therefore, the active damping technique is suitable for the LCL-filter system to mitigate the resonance and maintain the high efficiency. The filter-based active damping techniques without additional sensor have been presented in [4], [5], and the active damping techniques by the filter capacitor current feedback are presented in [6]–[18]

The authors would like to thank Ministry of Science and Technology, Taiwan for their financial supports in this research (104-2221-E-007-045-MY3).

The behavior of long transmission cable in offshore wind farm is modeled as a multiple series-connection π -equivalent circuits [19], [20]. As a result, the long transmission cable leads to several resonance frequencies in the system. The filter-based active damping techniques [4], [5] only suppress the resonance of the LCL filter, and thus it cannot be suitable for a multiple resonance frequencies system. In addition, the sampling delay and modulation delay decrease the phase margin of the system and reduces the effectiveness of the active damping technique [21]. The conventional control stability analysis only focuses on the internal current control loop from the current command to the output current. However, because the resonance occurred between the grid impedance and the current controller is not considered, it results in unpredictable resonance in the system [22], [23]. Therefore, the passivity-based stability analysis, so-called as the external stability analysis, is presented to estimate the overall system stability. The grid impedance is important to estimate the external stability, but the techniques in [6], [7] are only worked in a strong-grid system ignoring the grid impedance. Although the active damping techniques in [8]–[18] include a single inductive grid impedance, the characteristics of multiple resonance frequency on long transmission cable and multi-paralleled converter are not considered.

This paper provides an active damping method based on the virtual resistor technique with the filter capacitor current feedback. Comparing to literature papers, this paper identifies the proposed active damping technique by analyzing both of the internal and external stability on the Danish offshore wind farm application (Horns Rev offshore wind farm [24]). Besides, the behaviors of long transmission line and the multi-paralleled converter system are studied in this paper. The simulation results are used to verify the offshore wind farm system applications, and the laboratory experiment results demonstrate a down-scaled converter system to verify the proposed method.

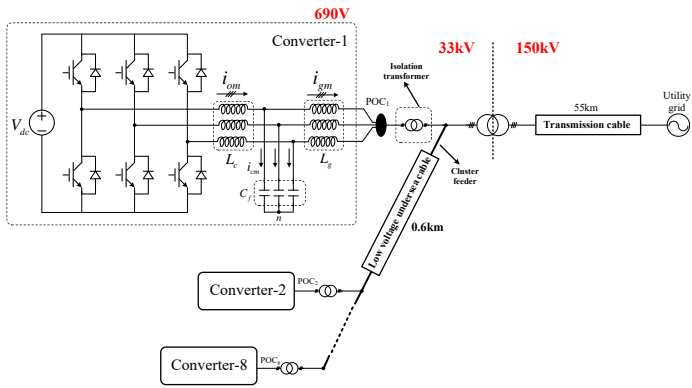


Fig. 1. The system configuration of an offshore wind farm.

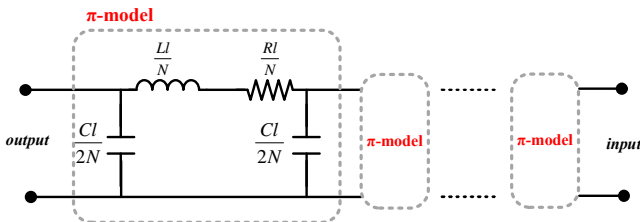


Fig. 2. The equivalent π -model of the transmission cable.

II. CONTROL BLOCK DIAGRAM AND THE SYSTEM CONFIGURATION

A. Offshore wind farm system

The Horns Rev 160MW offshore wind farm in Denmark [24] is an example for the stability estimation in this paper. Fig. 1 is the system configuration of the offshore wind farm. The wind power converters are paralleled in the low voltage side of the 33kV-bus through a 0.6km low voltage undersea transmission cable, and then the system connects to the utility grid through a 5km high voltage transmission cable. The high voltage transmission cable includes a 34km onshore buried cable (X_{on}) and a 21km offshore cable (X_{off}). The length of the low voltage cable between each wind turbine is 0.66km (X_{tb}), and the paralleled-number of each feeder is 8. The parameters of the transmission cable are shown in TABLE I based on ABB high voltage cable user guideline. The two-level converter is employed in this paper, and the converter connects to the point of connecting (POC) through an LCL filter (L_c : converter-side filter inductor; C_f : filter capacitor; L_g : grid-side filter inductor).

TABLE I
THE PARAMETERS OF A THE TRANSMISSION CABLE

Cable	L (mH/km)	C (μ F/km)	R (Ω /km)	Number of π -model
X_{on}	0.55	0.271	0.0151	10
X_{off}	0.38	0.19	0.027	5
X_{tb}	0.44	0.18	0.18	1

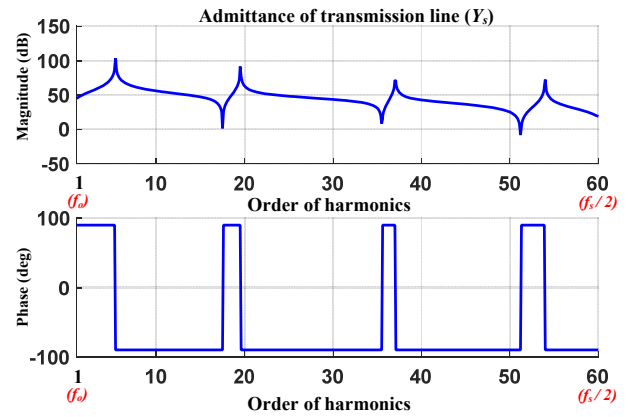


Fig. 3. The admittance of the transmission cable in frequency domain.

The power capacity of each wind power converter is 2.2MW, and it is operated at 2MW in normal operation, where the POC voltage is 50Hz and 690V (line-to-line; rms). The switching frequency is 2850 Hz, and the sampling frequency (f_s) is 5700Hz. In general cases, the filter is designed to manage the maximum peak-to-peak current ripple between 17% to 50% [25]–[27]. In this paper, the maximum peak-to-peak current ripple is 28.5%, and then the LCL parameters are: $L_c = 109\mu$ H (16%), $C_f = 1.67$ mF (11.2%), and $L_g = 40.9\mu$ H (6.5%; including the leakage inductance of the isolation transformer). Notice that the damping resistor of the LCL filter is removed in order to intensify the resonance in the system.

B. Long transmission cable modeling

To emulate the performance of the long transmission cable in frequency domain, the equivalent π -model is given by Equation (1) [19], [20] and shown in Fig. 2.

$$f_{max} = \frac{N}{8 \cdot l \cdot \sqrt{LC}}, \quad (1)$$

where the f_{max} is set at the Nyquist frequency. The f_{max} is usually set at the half of the sampling frequency ($0.5f_s$), and l is the length of the transmission line. L and C are the inductance and the capacitance of the transmission cable per kilometers based on the manufacturer, respectively. Therefore, the number of π -model sections (N) can thus be calculated by Equation (1).

Fig. 3 shows the overall admittance of the offshore and the onshore transmission cables, where the number of the π -model of the offshore and onshore cable is 5 and 10, respectively. Notice that the scale of the x-axis is the order of the harmonics from 1st (grid frequency; 50Hz) to 60th (3000Hz). Comparing to the conventional simple inductive cable system, the cascaded equivalent π -model emulates the multiple resonance frequencies in high frequency. Therefore, the characteristic of multiple resonance frequencies in real transmission cable is considered, and then it is employed to estimate the system stability.

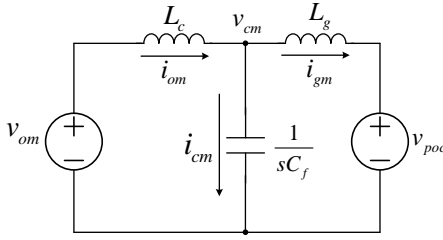


Fig. 4. The equivalent circuit of the LCL-filter.

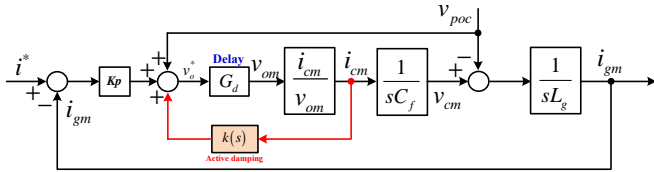


Fig. 5. The control block diagram of the current control and the active damping technique.

C. Overall control block diagram

Fig. 4 is the equivalent circuit of the LCL filter. Fig. 5 shows the block diagram of the current controller and the active damping technique, where the $k(s)$ is the loop gain of the proposed active damping technique. The proportional current control with a feedforward is employed to secure the grid-side current control, where K_p is the parameter of the proportional gain. The transfer function of i_{cm}/v_{om} is calculated as:

$$\frac{i_{cm}}{v_{om}} = \frac{L_g C_f s}{L_c + L_g + L_c L_g C_f s^2} \quad (2)$$

The sampling delay and modulation delay are respectively 1 and 0.5 times of sampling period (T_s) [28], [29], so that the overall delay is expressed as

$$G_d = e^{-1.5T_s s}. \quad (3)$$

III. THE PROPOSED VIRTUAL RESISTOR TECHNIQUE

This paper provides a virtual resistor technique to mitigate the resonance of the LCL filter. Fig. 6(a) shows the equivalent circuit with the passive resistor damping (R_v), and Fig. 6(b) shows the equivalent circuit with the proposed virtual resistor technique. As shown in Fig. 5, the proposed active damping technique obtains the filter capacitor current (i_{cm}) with $k(s)$ to emulate R_v . The filter capacitor current is calculated by the grid-side and converter-side inductor currents:

$$i_{cm} = i_{om} - i_{gm}. \quad (4)$$

Based on Fig. 6(a), the transfer function of the equivalent admittance looking from the point of the v_{om} is calculated as

$$\frac{i_{om}}{v_{om}} = \frac{1 + C_f R_v s + C_f L_g s^2}{s(L_c + L_g + C_f L_c R_v s + C_f L_g R_v s + C_f L_c L_g s^2)}. \quad (5)$$

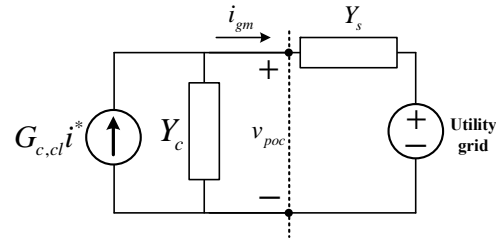


Fig. 7. The equivalent circuit of converter and the controller for passivity-based stability analysis.

On the other hand, the transfer function of the equivalent admittance looking from the point of the v_{om} based on Fig. 6(b) is calculated as

$$\frac{i_{om}}{v_{om}} = \frac{1 + C_f L_g s^2}{s(L_c + L_g - C_f L_g k(s)s + C_f L_c L_g s^2)}. \quad (6)$$

The admittance in Equation (5) and Equation (6) are equal in order to mimic the R_v by $k(s)$. Thus, the $k(s)$ can be calculated as

$$k(s) = -\frac{C_f L_g R_v s^2}{C_f L_g s^2 + C_f R_v s + 1}. \quad (7)$$

The proposed active damping technique is implemented in the DSP, the backward transform functions is employed for s to z domain:

$$s = \frac{f_s(z-1)}{z}, \quad (8)$$

where f_s is the sampling frequency.

IV. STABILITY ANALYSIS OF THE PROPOSED ACTIVE DAMPING CONTROL

A. Passivity-based stability analysis

The passivity-based stability analysis has been widely applied to estimate the system external stability, and it is employed in this paper. Based on Fig. 5, the output grid-side inductor current is expressed as

$$i_{gm} = G_{c,cl} \cdot i^* + Y_c \cdot v_{poc}, \quad (9)$$

where

$$G_{c,cl} = \left. \frac{i_{gm}}{i^*} \right|_{v_{poc}=0}, \quad Y_c = \left. \frac{i_{gm}}{v_{poc}} \right|_{i^*=0}. \quad (10)$$

Fig. 7 is the equivalent circuit of Equation (9). Y_s is the outside equivalent admittance looking from the POC. The $G_{c,cl}$ is the closed-loop gain of the current control, and the stability of $G_{c,cl}$ can be analyzed by the open-loop gain $G_{c,op}$. The Y_c is the admittance of the converter, and the external stability of the system is related to the Y_c and Y_s . Based on the definition of Y_c in Equation (10), the Y_c can be calculated as Equation (11) based on Fig. 8.

$$G_{c,cl} = \frac{K_p G_d X_{Cf} \frac{i_{cm}}{v_{om}}}{X_{Lg} - X_{Lg} G_d k(s) \frac{i_{cm}}{v_{om}} + K_p G_d X_{Cf} \frac{i_{cm}}{v_{om}}}, \quad Y_c = \frac{-G_d(k(s) + X_{Cf}) + X_{Cf} + X_{Lc}}{G_d(K_p X_{Cf} - k(s)X_{Lg}) + X_{Cf}(X_{Lc} + X_{Lg}) + X_{Lc}X_{Lg}}, \quad (11)$$

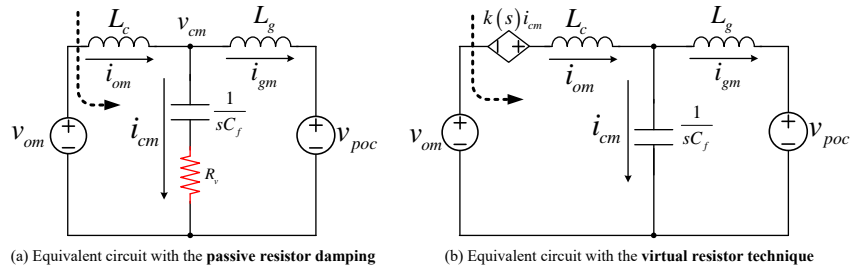


Fig. 6. The equivalent circuit of the LCL-filter with the R_v and the proposed active damping.

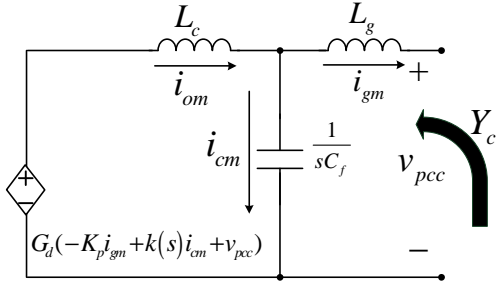


Fig. 8. The equivalent circuit of Y_c calculation.

where

$$X_{Lc} = sL_c, \quad X_{Lg} = sL_g, \quad \text{and} \quad X_{Cf} = \frac{1}{sC_f}.$$

Based on the literature [23], the system resonance will be amplified as

- The magnitude of Y_c and Y_s are equal, and the image-part of the Y_c and Y_s are opposite (resonance characteristic).
- One of the phase degree of Y_c or Y_s is located over 90° or below -90° (negative real-part of the admittance).

In the above case, the equivalent circuit is looked like an RLC circuit with a negative damping factor. Consequently, the resonance is amplified and thus leads to huge output current distortion. Based on this reason, the external stability analysis takes both of the Y_c and Y_s into account.

Based on the above discussion, the system includes the internal stability and external stability. The internal stability is used to ensure the current control loop is stable, and the external stability is employed to identify the resonance between the grid impedance and the converter. The stable system is that the internal control loop is stable, and both of Y_c and Y_s are passivity at all of the resonance frequencies.

B. The stability analysis of single-converter system

1) *Internal stability analysis:* To ensure the stable of the current control loop ($G_{c,cl}$) is the first step to estimate the system stability. Therefore, Fig. 9 shows the bode diagram of the open-loop current controller, where the proposed active damping technique is active in $G'_{c,op}$. As a result, both of the $G_{c,op}$ and $G'_{c,op}$ are stable (gain-margin > 0 and phase-margin > 0).

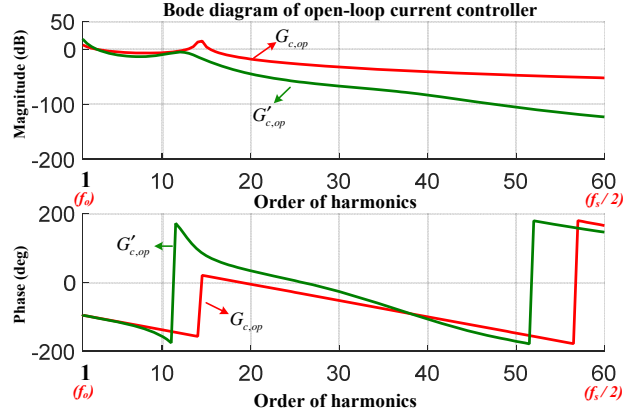


Fig. 9. The bode diagram of the open-loop current controller ($G_{c,op}$ and $G'_{c,op}$).

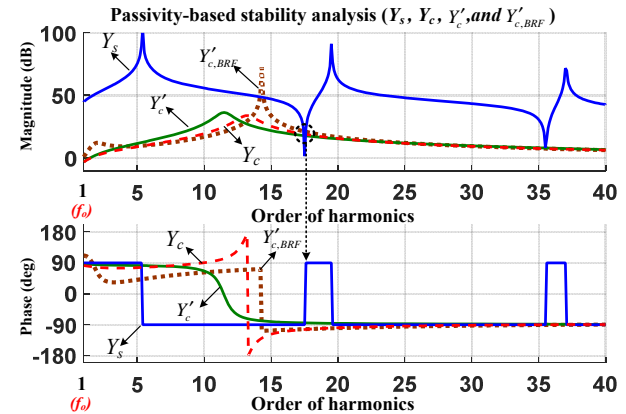


Fig. 10. The passivity-based analysis of the Y_s , Y_c , Y'_c , and $Y'_{c,BRF}$ in the single-converter system ($R_v = 500\Omega$).

2) *External stability analysis:* Based on Equation (1) and the transmission cable parameters in TABLE I, the admittance of the transmission cable Y_s in frequency domain is shown in Fig. 3. As a result, the inductor and capacitor in equivalent cascaded π -model lead to multiple resonance frequencies in 5.4th, 19.5th, 37th, and 54th order of harmonics.

Based on Equation (11), Fig. 10 illustrates the admittance of Y_s , Y_c , Y'_c , and $Y'_{c,BRF}$ in frequency domain, where the active damping is disable in Y_c , the proposed active damping is active

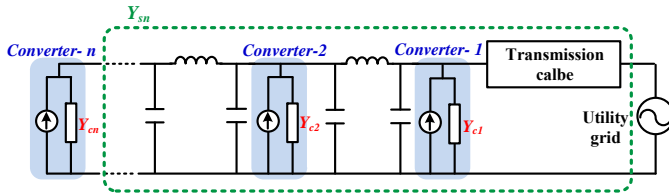


Fig. 11. The equivalent circuit of a multiple parallel-converter system.

in Y'_c , and the previous band-reject filter (BRF) active damping is employed in $Y'_{c,BRF}$ [4], [5]. The resonance frequency (ω_{res}) of the LCL-filter is at 14.3th order of harmonic, so that the BRF-based active damping sets the rejection frequency and the bandwidth at ω_{res} and $0.1\omega_{res}$, respectively.

The multiple resonance frequency of long transmission cable leads to several cross-points as shown in Fig. 10, which are the resonance points of the overall system. As a result, although the conventional BRF-based technique prevents the resonance at 14.3th order of harmonic, the resonance will be amplified by the negative real-parts of the $Y'_{c,BRF}$ at the next resonance frequency (17.5th order of harmonic). Besides, the analysis also illustrates the proposed active damping technique regulates the real-part of equivalent admittance Y'_c to the positive-region. Therefore, the resonance will be mitigated by the proposed method. These analysis will be verified by the simulation results in Section V-A.

C. The stability analysis of multiple parallel-converter system

The multi-paralleled converter system is illustrated at Fig. 1, and an 8-parallel converter system is analyzed in this section. Based on Fig. 7, each converter and the current controller can be expressed as a current source paralleled with an admittance. Thus, the multiple-parallel system in Fig. 1 can be simplified as Fig. 11 for the passivity-based stability analysis. To ensure the stable system operation in the last converter of the system is an index to estimate the overall system stability since the plant admittance (Y_{c8} ; the equivalent grid admittance of converter-8) includes all the other parallel-converters and the transmission cable.

Fig. 12 shows the admittance analysis of the last converter in the system (Y_{s8} and Y_{c8}). As a result, the resonance frequencies are not located at the negative real-part region of the Y_{c8} . Therefore, the last power converter is stable and without the amplified resonance in the 8-paralleled converter system.

V. SIMULATION AND LABORATORY EXPERIMENT RESULTS

A. Simulation results

The system configuration of an offshore wind power farm is shown in Fig. 1, and the control block diagram is shown in Fig. 4. Fig. 13 is the previous BRF-based active damping technique [4], [5] employed to identify the performance in the offshore wind farm applications. The parameters of the transmission cable and the equivalent π -model are shown in TABLE I and Fig. 2, respectively. The K_p in grid-side current

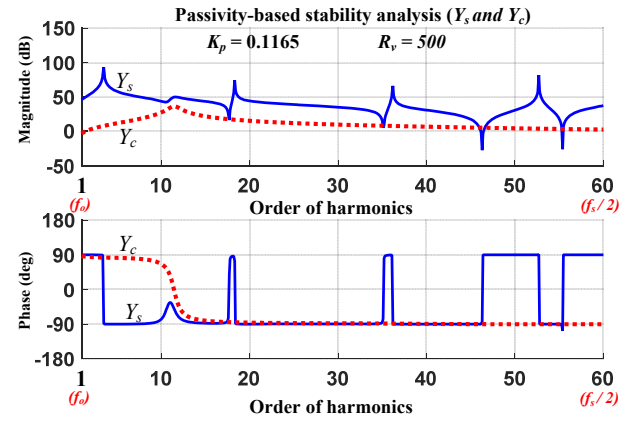


Fig. 12. The admittance of the Y_c and Y_s with the active damping technique in multiple parallel-converter system ($R_v = 500\Omega$).

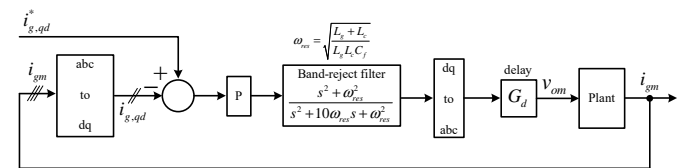


Fig. 13. The control block diagram of the previous filter-based active damping.

controller is set at 0.1165, and the R_v is set at 500Ω . The passivity-based stability analysis of both single-converter and multiple parallel-converter systems are discussed and analyzed in Section IV-A.

Fig. 14 illustrates the output currents waveform under a single wind power converter system under the operation with/without the proposed method and BRF-based active damping. As a result, the resonance is triggered and amplified as the active damping technique is disable at $t = 0.1s$. In addition, Fig. 15 illustrates the simulation results under an 8-paralleled converter system. As a result, the resonance is mitigated in the system and the controller secures the stable without the amplified resonance.

The simulation results verify the passivity-based stability analysis in Section IV-A. Based on Fig. 10 and Fig. 14, the resonance is amplified by the negative real-part of the Y_c and $Y'_{c,BRF}$ when the system without the proposed active damping technique. Moreover, the proposed method prevents the resonance in the system even though the system is a multi-paralleled converter system.

B. Laboratory experiment results

The system configuration of the laboratory experiment results is shown in Fig. 17, where the grid impedance L_s is 0.45mH. In order to emulate the system operated at the difference operation point and the parameters, two converters are tested and the parameters of the LCL filter and controller are shown in TABLE II.

Fig. 18 illustrates the stability analysis of the converter-

TABLE II
THE PARAMETERS OF A THE LABORATORY TEST BENCH

Parameters	L_c	L_g	C_f	T_s	R_w	K_p	Rated power
Converter-1	3.3mH	2.2mH	9.2 μ F	1/10ms	500 Ω	13	3.3kW
Converter-2	2.2mH	1mH	20 μ F	1/10ms	500 Ω	7	3.3kW

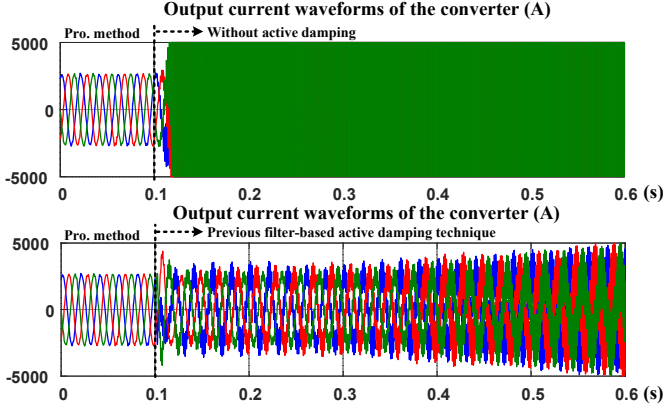


Fig. 14. The simulation result in a single wind power converter system.

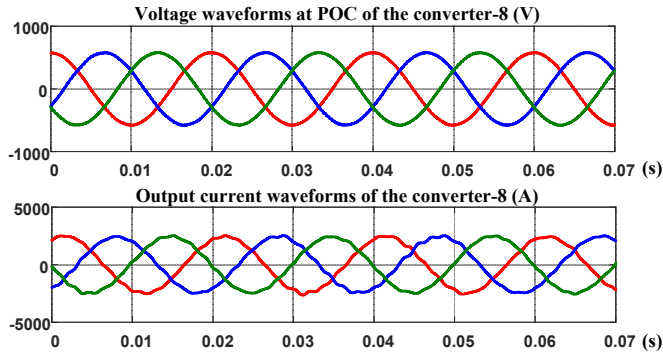


Fig. 15. The simulation result under the system in Fig. 1.

1, where Y_{cl} and Y'_{cl} are the equivalent control admittance excluding and including the proposed method, respectively. Based on the analysis, the resonance in converter-1 is triggered as the active damping technique is disabled, and the proposed active damping technique regulates the phase to the passivity region. Fig. 19 verifies the analysis by the laboratory experiment results, which significantly shows the resonance is

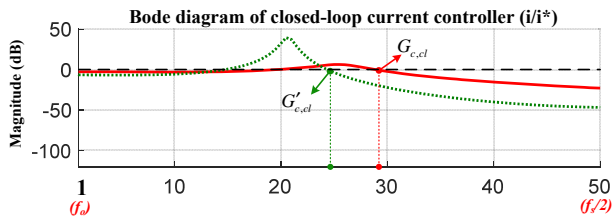


Fig. 16. The magnitude of the closed-loop current controller on converter-1.

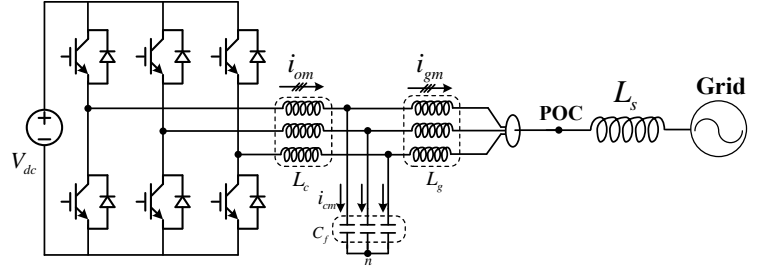


Fig. 17. The system configuration for laboratory experiment verification.

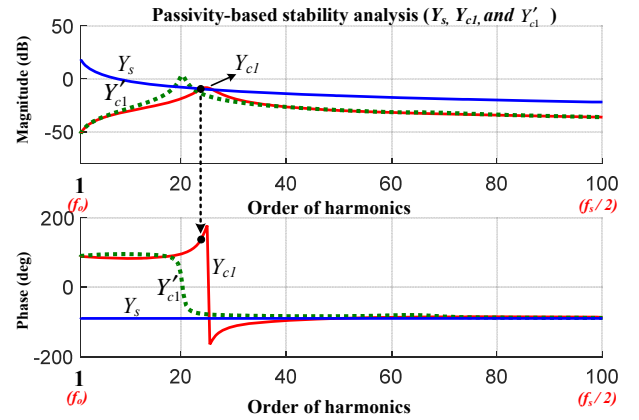


Fig. 18. The passivity-based stability analysis under a single converter-1 system.

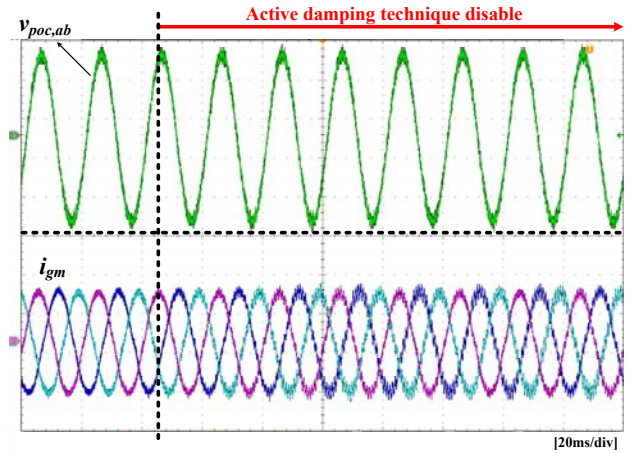


Fig. 19. The laboratory experiment result under a single converter-1 system ($v_{poc,ab}$: 250V/div; i_{gm} : 10A/div).

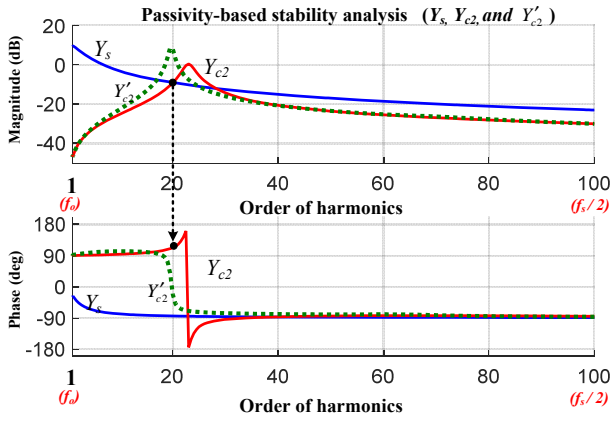


Fig. 20. The passivity-based stability analysis under a single converter-2 system.

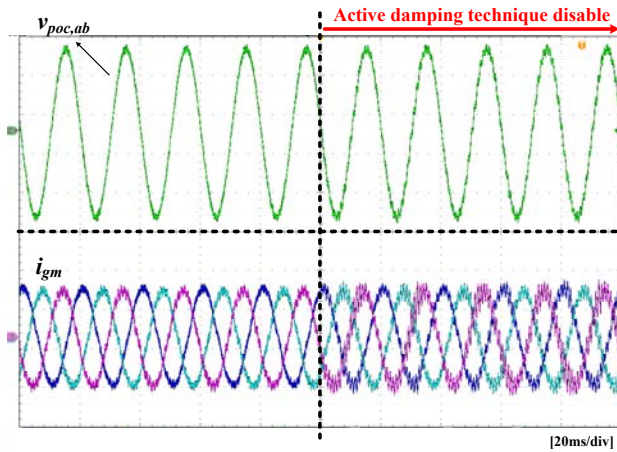


Fig. 21. The laboratory experiment result under a single converter-2 system ($v_{poc,ab}$: 250V/div; i_{gm} : 10A/div).

amplified as the proposed method is disable.

Fig. 20 shows the stability analysis of the converter-2. The cross-point of Y_{c2} and Y_s is in the negative real-part region of the Y_{c2} . Notice that the cross-point of Y_{c2}' and Y_s is very closed to the boundary of 90° , which means the the operation is very closed to the resonance region. Fig. 21 shows the output current has a slight current distortion even though the active damping is active, and then the resonance is significantly amplified as the active damping technique is disable.

VI. DYNAMIC PERFORMANCE AND R_v REGULATION ANALYSIS

A. Current control dynamic analysis

The dynamic performance is one of the requirements of the wind power converters. As shown in Fig. 7, the output current control is managed by a independent current source ($G_{c,cl}$). The corner frequency of the closed-loop gain is an index to estimate the dynamic of the current control. Fig. 16 shows the bode diagram analysis based on the parameters of the converter-1 in TABLE II. $G_{c,cl}$ is the closed-loop gain without the proposed active damping, and the proposed

active damping technique is active at $G'_{c,cl}$. As a result, the proportional current control leads to the steady-error, and the steady-state error of the $G'_{c,cl}$ is larger than the $G_{c,cl}$. Besides, the bandwidth of $G_{c,cl}$ is higher than $G'_{c,cl}$ (115% of the $G'_{c,cl}$), which means the dynamic performance of $G_{c,cl}$ is faster.

Based on the analysis, the proposed method improves the external system stability, but it also increases the steady-state error and decreases the control bandwidth.

B. The stability of R_v regulation

The proportional grid-side inductor current control is employed in this paper. The proportional gain is designed based on the desired current control bandwidth β_{bw} , where the control bandwidth is usually set at 10% of the sampling frequency [30]:

$$\beta_{bw} \leq \frac{2\pi f_s}{10}, \text{ and } K_p = \beta_{bw} L_g \quad (12)$$

Fig. 22 shows the bode diagram of the Y_{c1} with the R_v regulation based on the parameters of converter-1 in TABLE II. As a result, the passivity region of Y_{c1} increases as R_v becomes higher. Besides, the frequency performance of Y_{c1} in R_v is 50 and 500 are similar, which illustrates that the Y_{c1} performance has the saturation characteristic. The large R_v ($R_v \gg 2\sqrt{L_g/C_f}$), the $k(s)$ in Equation (7) can be simplified as

$$k(s) = \frac{-R_v s}{s + R_v/L_g}. \quad (13)$$

As a result, the performance of $k(s)$ can be looked like a high-pass filter with $-R_v$ gain, and this saturation characteristic help for the user design.

Fig. 23 is the bode diagram of the open-loop current control ($G_{c,op}$) with the R_v regulation based on the parameters of converter-1 in TABLE II. As a result, the phase margin is improved as the R_v increases, which illustrates the stability of the system is increased.

Based on above analysis, the proposed active damping technique increases both of the internal and external system stability. The maximum external stability region of the system can be estimated by selecting a large R_v , i.e. $R_v = 4\sqrt{L_g/C_f}$, based on the saturation characteristic.

VII. CONCLUSION

The LCL filter increases the risk of the amplified resonance to disturb the system stability, where the amplified resonance is occurred by not only the LCL filter (internal resonance) but also the interaction between the current controller and the equivalent grid impedance (external resonance). This paper provides a virtual-resistor-based active damping technique to reduce the risk of amplified resonance.

Comparing to the conventional stability analysis only focused on the internal LCL resonance suppression, the passivity-based stability analysis is employed in this paper to estimate the overall system stability. To emulate the proposed method in a wind farm system applications, the behavior of the long transmission cable and the multiple parallel-converter

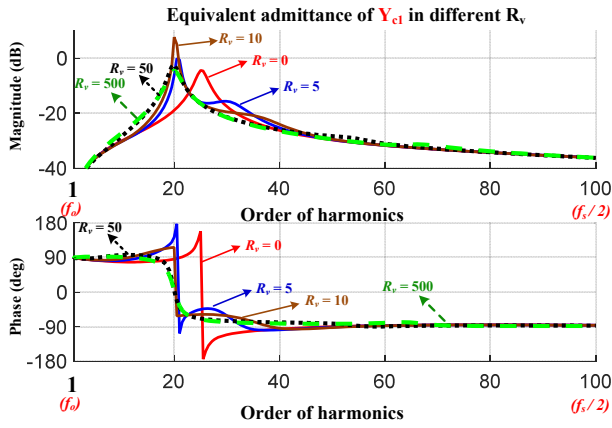


Fig. 22. The bode diagram of the Y_{ci} in different R_v .

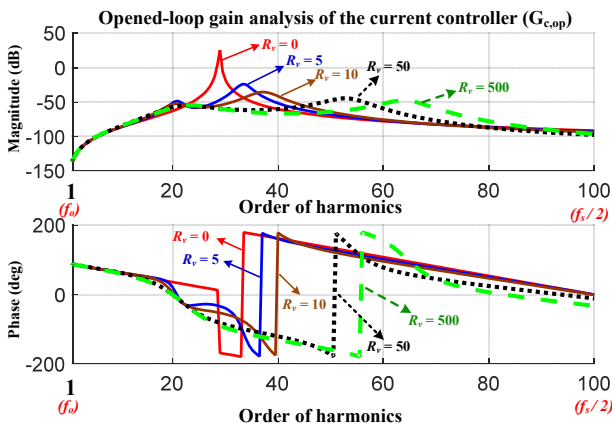


Fig. 23. The bode diagram of the $G_{c,op}$ in different R_v .

are taken into the stability analysis. The simulation results verify the proposed method in a Danish offshore wind farm system, and the down-scaled system is verified in the laboratory experiment results. Finally, the dynamic and the R_v selection are compared and discussed in the paper.

REFERENCES

- [1] R. Teodorescu, F. Blaabjerg, M. Liserre, and A. Dell'Aquila, "A stable three-phase lcl-filter based active rectifier without damping," in *Industry Applications Conference, 2003. 38th IAS Annual Meeting. Conference Record of the*, vol. 3. IEEE, 2003, pp. 1552–1557.
- [2] M. Liserre, F. Blaabjerg, and S. Hansen, "Design and control of an lcl-filter-based three-phase active rectifier," *IEEE Transactions on Industry Applications*, vol. 41, no. 5, pp. 1281–1291, 2005.
- [3] W. Gullvik, L. Norum, and R. Nilsen, "Active damping of resonance oscillations in lcl-filters based on virtual flux and virtual resistor," in *Power Electronics and Applications, 2007 European Conference on*. IEEE, 2007, pp. 1–10.
- [4] J. Dannehl, M. Liserre, and F. W. Fuchs, "Filter-based active damping of voltage source converters with lcl filter," *IEEE Transactions on Industrial Electronics*, vol. 58, no. 8, pp. 3623–3633, 2011.
- [5] W. Yao, Y. Yang, X. Zhang, and F. Blaabjerg, "Digital notch filter based active damping for lcl filters," in *Applied Power Electronics Conference and Exposition (APEC), 2015 IEEE*. IEEE, 2015, pp. 2399–2406.
- [6] J. Dannehl, F. W. Fuchs, S. Hansen, and P. B. Thøgersen, "Investigation of active damping approaches for pi-based current control of grid-connected pulse width modulation converters with lcl filters," *IEEE*

- Transactions on Industry Applications*, vol. 46, no. 4, pp. 1509–1517, 2010.
- [7] J. He and Y. W. Li, "Generalized closed-loop control schemes with embedded virtual impedances for voltage source converters with lcl or lcl filters," *IEEE Transactions on Power Electronics*, vol. 27, no. 4, pp. 1850–1861, 2012.
- [8] Y. Tang, P. C. Loh, P. Wang, F. H. Choo, F. Gao, and F. Blaabjerg, "Generalized design of high performance shunt active power filter with output lcl filter," *IEEE Transactions on Industrial Electronics*, vol. 59, no. 3, pp. 1443–1452, 2012.
- [9] W. Li, X. Ruan, D. Pan, and X. Wang, "Full-feedforward schemes of grid voltages for a three-phase-type grid-connected inverter," *IEEE Transactions on Industrial Electronics*, vol. 60, no. 6, pp. 2237–2250, 2013.
- [10] D. Pan, X. Ruan, C. Bao, W. Li, and X. Wang, "Capacitor-current-feedback active damping with reduced computation delay for improving robustness of lcl-type grid-connected inverter," *IEEE Transactions on Power Electronics*, vol. 29, no. 7, pp. 3414–3427, 2014.
- [11] Z. Xin, P. C. Loh, X. Wang, F. Blaabjerg, and Y. Tang, "Highly accurate derivatives for lcl-filtered grid converter with capacitor voltage active damping," *IEEE Transactions on Power Electronics*, vol. 31, no. 5, pp. 3612–3625, 2016.
- [12] X. Wang, C. Bao, X. Ruan, W. Li, and D. Pan, "Design considerations of digitally controlled lcl-filtered inverter with capacitor-current-feedback active damping," *IEEE Journal of Emerging and Selected Topics in Power Electronics*, vol. 2, no. 4, pp. 972–984, 2014.
- [13] R. Peña-Alzola, M. Liserre, F. Blaabjerg, M. Ordóñez, and Y. Yang, "Lcl-filter design for robust active damping in grid-connected converters," *IEEE Transactions on Industrial Informatics*, vol. 10, no. 4, pp. 2192–2203, 2014.
- [14] D. Pan, X. Ruan, C. Bao, W. Li, and X. Wang, "Optimized controller design for lcl-type grid-connected inverter to achieve high robustness against grid-impedance variation," *IEEE Transactions on Industrial Electronics*, vol. 62, no. 3, pp. 1537–1547, 2015.
- [15] X. Li, X. Wu, Y. Geng, X. Yuan, C. Xia, and X. Zhang, "Wide damping region for lcl-type grid-connected inverter with an improved capacitor-current-feedback method," *IEEE Transactions on Power Electronics*, vol. 30, no. 9, pp. 5247–5259, 2015.
- [16] X. Wang, F. Blaabjerg, and P. C. Loh, "Virtual rc damping of lcl-filtered voltage source converters with extended selective harmonic compensation," *IEEE Transactions on Power Electronics*, vol. 30, no. 9, pp. 4726–4737, 2015.
- [17] D. Pan, X. Ruan, and X. Wang, "Direct realization of digital differentiators in discrete domain for active damping of lcl-type grid-connected inverter," *IEEE Transactions on Power Electronics*, 2017.
- [18] A. Aapro, T. Messo, T. Roinila, and T. Suntio, "Effect of active damping on output impedance of three-phase grid-connected converter," *IEEE Transactions on Industrial Electronics*, vol. 64, no. 9, pp. 7532–7541, 2017.
- [19] M. Khatir, S. Zidi, S. Hadjeri, and M. K. Fellah, "Comparison of hvdc line models in psb/simulink based on steady-state and transients considerations," *Acta Electrotechnica et Informatica*, vol. 8, no. 2, pp. 50–55, 2008.
- [20] M. Zubiaga, G. Abad, J. Barrena, S. Aurtenetxea, and A. Cárcar, "Spectral analysis of a transmission system based on ac submarine cables for an offshore wind farm," in *Industrial Electronics, 2009. IECON'09. 35th Annual Conference of IEEE*. IEEE, 2009, pp. 871–876.
- [21] M. Lu, X. Wang, P. C. Loh, F. Blaabjerg, and T. Dragicevic, "Graphical evaluation of time-delay compensation techniques for digitally controlled converters," *IEEE Transactions on Power Electronics*, vol. 33, no. 3, pp. 2601–2614, 2018.
- [22] L. Harnefors, A. G. Yepes, A. Vidal, and J. Doval-Gandoy, "Passivity-based controller design of grid-connected vscs for prevention of electrical resonance instability," *IEEE Transactions on Industrial Electronics*, vol. 62, no. 2, pp. 702–710, 2015.
- [23] X. Wang, F. Blaabjerg, and P. C. Loh, "Passivity-based stability analysis and damping injection for multiparalleled vscs with lcl filters," *IEEE Transactions on Power Electronics*, vol. 32, no. 11, pp. 8922–8935, 2017.
- [24] P. Christiansen, K. K. Jørgensen, and A. G. Sørensen, "Grid connection and remote control for the horns rev 150 mw offshore wind farm in denmark," in *Proceedings of the 2nd International Workshop on Transmission Networks for Offshore Wind Farms*, 2000, pp. 29–30.

- [25] U. Rädcl, "Beitrag zur entwicklung leistungselektronischer komponenten für windkraftanlagen," Ph.D. dissertation, Dissertation, Ilmenau, 2008.
- [26] J. M. Bloemink and T. C. Green, "Reducing passive filter sizes with tuned traps for distribution level power electronics," in *Power Electronics and Applications (EPE 2011), Proceedings of the 2011-14th European Conference on*. IEEE, 2011, pp. 1-9.
- [27] K. R. Meyer, "Fault-ride-through-regelung von windenergieanlagen mit vollumrichter und lcl-netzfilter," Ph.D. dissertation, 2014.
- [28] S. Buso and P. Mattavelli, "Digital control in power electronics," *Lectures on power electronics*, vol. 1, no. 1, pp. 1-158, 2006.
- [29] D. M. VandeSype, K. DeGusseme, F. M. DeBelie, A. P. VandenBossche, and J. A. Melkebeek, "Small-signal z-domain analysis of digitally controlled converters," *IEEE Transactions on Power Electronics*, vol. 21, no. 2, pp. 470-478, 2006.
- [30] L. Harnefors and H.-P. Nee, "Model-based current control of ac machines using the internal model control method," *IEEE transactions on industry applications*, vol. 34, no. 1, pp. 133-141, 1998.



Hsin-Chih Chen (S'12) received the B.S. degree in Electrical Engineering at Feng Chia University, Taichung, Taiwan, in 2011 and the Ph.D. degree in Electrical Engineering at National Tsing Hua University, Hsinchu, Taiwan, in 2018.

His research interests include power electronics applications on distributed power systems, multilevel converter, and power converter controls. He was a guest Ph.D. student and worked on the control stability analysis in a multi-parallelled converter system supported by the Ministry of Science and

Technology, Taiwan, with the Professor Frede Blaabjerg on Department of Energy Technology, Aalborg University, Aalborg, Denmark, in 2018.

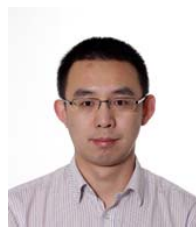
Dr. Chen received the International Conference on Power Electronics and ECCE Asia (ICPE 2015-ECCE Asia) Best Paper Award in 2015. He received the Energy Conversion Congress and Exposition (ECCE 2015) Best Poster Award in 2015.



Po-Tai Cheng (S'96-M'99-SM'09-F'18') received the B.S. degree from National Chiao Tung University, Hsinchu, Taiwan, in 1990 and the Ph.D. degree from the University of Wisconsin-Madison, Madison, WI, USA, in 1999. He is currently a Professor with the Department of Electrical Engineering, National Tsing Hua University, Hsinchu, Taiwan.

His research interests include high-power converters and applications, and power electronics technologies for smart grid.

He received IAS Transactions Prize Paper Award in 2009 and IAS Industrial Power Converter Committee paper award in 2012 and 2014. He is the chairperson of the Industrial Power Conversion Systems Department, IAS, 2016-2017, and a member-at-large of the IAS Executive Board 2014-2015, 2018-2019. He also serves as a Distinguished Lecturer of IEEE PELS for 2014-2017, and an associate editor of IEEE TRANSACTIONS ON POWER ELECTRONICS.



Xiongfei Wang (S'10-M'13-SM'17) received the B.S. degree from Yanshan University, Qinhuangdao, China, in 2006, the M.S. degree from Harbin Institute of Technology, Harbin, China, in 2008, both in electrical engineering, and the Ph.D. degree in energy technology from Aalborg University, Aalborg, Denmark, in 2013. Since 2009, he has been with the Aalborg University, Aalborg, Denmark, where he is currently an Associate Professor in the Department of Energy Technology. His research interests include modeling and control of grid-connected converters,

harmonics analysis and control, passive and active filters, stability of power electronic based power systems.

Dr. Wang serves as an Associate Editor for the IEEE TRANSACTIONS ON POWER ELECTRONICS, the IEEE TRANSACTIONS ON INDUSTRY APPLICATIONS, and the IEEE JOURNAL OF EMERGING AND SELECTED TOPICS IN POWER ELECTRONICS. He is also the Guest Editor for the Special Issue Grid-Connected Power Electronics Systems: Stability, Power Quality, and Protection in the IEEE TRANSACTIONS ON INDUSTRY APPLICATIONS. He received the second prize paper award and the outstanding reviewer award of IEEE TRANSACTIONS ON POWER ELECTRONICS in 2014 and 2017, respectively, the second prize paper award of IEEE TRANSACTIONS ON INDUSTRY APPLICATIONS in 2017, and the best paper awards at IEEE PEDG 2016 and IEEE PES GM 2017. In 2018, he received the IEEE PELS Richard M. Bass Outstanding Young Power Electronics Engineer Award.



Frede Blaabjerg (S'86M'88SM'97F'03) was with ABB-Scandia, Randers, Denmark, from 1987 to 1988. From 1988 to 1992, he got the PhD degree in Electrical Engineering at Aalborg University in 1995. He became an Assistant Professor in 1992, an Associate Professor in 1996, and a Full Professor of power electronics and drives in 1998. From 2017 he became a Villum Investigator. He is honoris causa at University Politehnica Timisoara (UPT), Romania and Tallinn Technical University (TTU) in Estonia.

His current research interests include power electronics and its applications such as in wind turbines, PV systems, reliability, harmonics and adjustable speed drives. He has published more than 500 journal papers in the fields of power electronics and its applications. He is the co-author of two monographs and editor of 7 books in power electronics and its applications.

He has received 26 IEEE Prize Paper Awards, the IEEE PELS Distinguished Service Award in 2009, the EPE-PEMC Council Award in 2010, the IEEE William E. Newell Power Electronics Award 2014 and the Villum Kann Rasmussen Research Award 2014. He was the Editor-in-Chief of the IEEE TRANSACTIONS ON POWER ELECTRONICS from 2006 to 2012. He has been Distinguished Lecturer for the IEEE Power Electronics Society from 2005 to 2007 and for the IEEE Industry Applications Society from 2010 to 2011 as well as 2017 to 2018. In 2018 he is President Elect of IEEE Power Electronics Society.

He is nominated in 2014, 2015, 2016 and 2017 by Thomson Reuters to be between the most 250 cited researchers in Engineering in the world.